Chemical and mechanical analysis of tribofilms from fully formulated oils Part 1 – Films on 52100 steel

G. Pereira[1], A. Lachenwitzer[1], M. Kasrai[1], G. M. Bancroft[1], P. R. Norton*[1], M. Abrecht[2], P. U. P. A. Gilbert[2,3], T. Regier[4], R. I. R. Blyth[4] and J. Thompson[1]

The authors report, for the first time, a comprehensive chemical and mechanical characterisation of antiwear films prepared from a fully formulated oil that is commercially available. Wear increases substantially when using the fully formulated oil compared to using ZDDP alone. X-ray absorption near edge structure (XANES) spectroscopy at the P K- and L-edges, S K-edge, Mo L-edge, B K-edge, Ca L-edge, O K-edge and Fe and Zn L-edges permits chemical characterisation of the major elements in the thin films. Ca phosphates, ZnS and MoS_2 are the main P and S species formed, contrary to previous studies involving only ZDDPs, whereby Zn phosphates are the dominant species. These findings can be accounted for by using the hard and soft acid and bases (HSAB) principle. Small amounts of $CaCO_3$ are present, but no B was detected, implying it does not become incorporated into the film. Atomic force microscopy (AFM) reveals continuous pads with a relatively uniform indentation moduli (125 ± 10 GPa), separated by trenches that are essentially comprised of uncovered steel substrate.

Keywords: Fully formulated oils, XANES, Mechanical properties, Antiwear film, Tribofilm

Introduction

Modern engine oil formulations contain a number of additives such as antiwear and extreme pressure additives, antioxidants, detergent dispersant packages, corrosion (rust) inhibitors, and both viscosity and friction modifiers. Each additive might affect the physical or chemical properties of either the metallic surface, or the base oil. However, there is a fundamental lack of understanding of the role each additive plays, based on the complexity that each additive component contributes to the overall mechanism.

The oxidation process involves reaction of the lubricant molecules with oxygen, and also the thermal decomposition at high temperatures. A free radical process ensues which propagates to form very acidic oxidation products, which increase the danger of corrosion. Antioxidants are added to engine oils to combat the radical propagation, and are classified into two groups, primary antioxidants (radical scavengers) and secondary antioxidants (peroxide decomposers).[1] The primary antioxidants form resonance stabilised radicals which inhibit the propagation step, and the secondary antioxidants prevent peroxides from chain branching.

Antiwear and extreme pressure additives have been extensively studied. They prevent wear caused by the cold welding of the moving parts. Wear can occur by many means, namely corrosion, metal to metal contact, or abrasion by solids and/or third bodies.[2] Antiwear additives are designed to reduce wear when the reciprocating surfaces are exposed to low to moderate pressures, while extreme pressure additives work in a more severe demanding environment.

Detergents and ashless dispersant packages are often added to engine oil formulations to keep oil–insoluble combustion products, and wear particles in suspension. Detergents are often overbased metal containing (typically calcium) compounds used to neutralise and suspend the acidic oxidation and combustion products.[1] Ashless dispersants are organic compounds used to keep oil–insoluble combustion products in solution.[1] Functioning as micelles, detergents and ashless dispersants suspend the four major classes of solubilisates which are sludge, sludge precursors, acids and water in engine oils.[3]

Corrosion of the engine surface has many causes, such as acidic thermal and oxidative byproducts of the lubricants, or environmental origins (water, water vapour, air). Corrosion inhibitors are divided into two categories, antirust additives which protect ferrous

[1]Department of Chemistry, University of Western Ontario, London, Ontario, N6A 5B7, Canada
[2]Synchrotron Radiation Center, University of Wisconsin, Stoughton, WI 53589, USA
[3]Physics Department, University of Wisconsin at Madison, Madison, WI 53706, USA
[4]Canadian Light Source Inc., University of Saskatchewan, 101 Perimeter Road, Saskatoon, SK, S7N 0X4, Canada

*Corresponding author, email pnorton@uwo.ca

Received 19 September 2006; accepted 5 March 2007
DOI 10.1179/175158407X189293

surfaces, and metal passivators for non-ferrous metals.[1] Both classes of inhibitors act in the same fashion, by competing to adsorb on the surface thereby reducing the efficiency of corrosion byproducts reaching the surface. This adsorption on the metal effectively reduces the efficiency of other additives, such as antiwear additives.

Another important factor of engine oils is the viscosity, η, or flow factor. Usually a low viscosity is needed during start-up and in cold climates. Today's after market oils for automobiles are multigrade oils, which typically contain organic polymers which are added to the oils that change the solubility strength with differing temperatures. This prevents the oil from excess thinning as it warms up. The Society of Automotive Engineers (SAE) designates arbitrary numbers to engine oils to describe the kinematic viscosity. For example, in a 5 W-30 engine oil, the 'W' means that the oil meets stipulations for viscosity at around -18°C (0 F) and is therefore suitable for winter use. The first number in the description of engine oil indicates the flow of the oil at cold temperatures, which in turn indirectly describes the chemical clustering behaviour of the polymer. The lower the first number, the better the flow at colder temperatures (i.e. 5 W oil can be pumped by your engine at a lower temperature than 10 W). The second number indicates the viscosity at optimal operating temperature. As the temperature increases, the solubility of the polymer improves, increasing viscosity and preventing the oil from thinning.

Friction modifying additives typically act at temperatures where antiwear additives are not yet reactive by forming a thin physically absorbed layer that exhibits a lower friction behaviour compared to other additives.[1] Typically, organomolybdenum compounds are used as friction modifying compounds that function by forming graphite-like MoS_2 sheets on the surface. The stacked layers are worn away and replaced, which results in protection of the surface.

The multifunctional additive, most prominent for its antioxidant, antiwear, and corrosion inhibition is a class of organometallic molecules called zinc dialkyl-dithiophosphates (ZDDPs). ZDDPs are known to break down under lubrication conditions to form a very thin (about 100–200 nm) amorphous polyphosphate film with varying chain lengths, which protects the surface by maintaining a physical barrier which is less stiff and softer than the substrate. This barrier, referred to as a tribofilm or antiwear film, is worn away, and reformed. This process reduces wear by acting as a sacrificial layer. ZDDPs are subject to many recent reviews which outline the necessity and importance of this class of molecules.[4–7] The phosphate glass that is formed is useful for protecting the engine. However, through the combustion process, some P containing contaminants end up being deposited on the catalytic converter elements, from which there is no effective way to remove them, effectively poisoning the catalyst. This results in a shorter lifetime of the converter, compensated by a higher catalytic metal loading which is why automakers are calling for a reduced amount of ZDDPs in engine oils. Meanwhile, the US Environmental Protection Agency (EPA) has progressively increased the duration of the mandatory warranties for the catalytic converter,[8] thus reducing the profit margin for manufacturers. In addition, the EPA's mandate is to reduce the phosphorus and sulphur pollutants being released into the environment, both elements being the main components of ZDDP.

Many studies have investigated the interaction of Ca based detergents and dispersants (phenates, sulfonates, salicylates) with ZDDPs.[9–17] The consensus is that the efficacy of ZDDPs is retarded through a competition of detergents and dispersants either absorbing on the surface or limiting the interaction between ZDDPs and the metal,[3,18,19] both routes resulting in antagonistic behaviour with respect to antiwear performance. Overbased detergents have also been shown to diminish the antioxidant properties of ZDDPs, while the more basic detergent seems to improve the frictional properties of the oil.[13] Through X-ray absorption near edge structure (XANES) spectroscopy it was found that upon addition of detergents, a decrease in polyphosphate chain length occurs which has been correlated to the poorer wear behaviour.[14,15] A very good synopsis of the interaction of ZDDPs with detergents and dispersants can be found in the literature.[5] The introduction of borated dispersants to ZDDPs has been investigated,[20] which show B in a trigonal geometry in the pristine additive. However, after rubbing, the geometry changes to tetrahedral coordination. Zhang *et al.*[20] have inferred from a multiedge XANES analysis that B is not integrated into the polyphosphate network, but is present inadvertently within the film.

The relationship between friction modifying additives with ZDDPs have also been subject to assorted studies. De Barros *et al.*[21] have shown that the antiwear action of ZDDPs when mixed with friction modifying molybdenum dithiocarbamate (MoDTC) produces a short chain polyphosphate in addition to ZnS, MoS_2 and various Mo oxides. MoDTCs function as both antiwear and extreme pressure additives, which are added to fully formulated oils which consequently reduce friction and gasoline consumption.[22]

Commercial lubricating oils contain a number of multifunctional additives, either purchased as packages or formulated for desired specificity. The synergistic or antagonistic chemical interactions between two component additive systems are well documented; however, engine oils formulations contain many kinds of additives, and the actions and properties each of these additives exhibit are expected to be different from single or dual additive systems, due to the mutual and competing interactions.

X-ray absorption near edge structure and X-ray photoelectron emission microscopy (X-PEEM) are surface analytical techniques which make use of a synchrotron radiation source.[23] The studies pertinent to the applications involve soft X-ray excitation of core level electrons, using a photoabsorption detection technique. The narrow core level edges that can be studied in the soft X-ray region are: the 1s (K-edge) of light elements from Li to Ar, and 2p (L-edge) of elements from Na to Zn, and the 3d (M-edge) of many heavier elements. This non-destructive technique has been used extensively in the past to investigate tribochemistry composition of antiwear films.[5,14,15,19,20] The majority of chemical speciation has been done at the P and S K- and L-edges. However, since the inception of the Canadian Light Source (CLS) Inc.'s spherical grating monochromator (SGM) and plane

grating monochromator (PGM) beamlines,[24] the authors are now capable of optimal chemical characterisation at high resolution of all the major elements present in commercial oils, which have core level edges between 40 and 1900 eV (Al, P, S, Mo, B, C, Ca, O, Fe and Zn).

Instrumented imaging nanoindentation has provided a useful tool to estimate the mechanical properties of antiwear films.[25–30] A synopsis of the present instrumentation can be found elsewhere.[31] Intuitively, if the antiwear pads are less stiff than the metals in contact, the surfaces are protected. The indentation moduli of antiwear pads are typically between 30 and 90 GPa, depending on the location (i.e. valley or ridge) and additive composition used to generate the films.

This study has undertaken the sizeable task of performing what the authors believe is the first examination of the chemistry and mechanical properties of tribofilms formed from fully formulated oils. The authors focus on the interactions of a fully formulated oil with 52100 steel, while the results obtained on an Al/Si alloy will be presented in Part 2 of this study.

Experimental

Materials, composition of substrate and sample preparation

The steel disks were toughened, quenched and hardened to $\sim$60 Rockwell C. The pins were treated in the same manner, and were used as-is. The steel samples were manufactured from 52100 steel rods into circular disks at the University of Western Ontario with dimensions of 10×4 mm. The composition of 52100 steel is approximately 1%C, 0·025%P, 0·025%S, 0·25%Si, 0·25–0·45%Mn, 1·3–1·6%Cr, and the balance as Fe.[32] The disks were subsequently mechanically polished with a 6, 3 and finally 0·5 μm diamond pastes using turpentine solvent. They were washed with methanol in an ultrasonic bath and stored to dry. The average surface roughness R_a and the root mean squared roughness R_{RMS} was found to be 8 ± 1 and 14 ± 4 nm respectively.

Model compounds, antiwear film preparation and coefficient of friction

Antiwear films were made on the polished, 52100 steel disks in a Plint high frequency wear tester. The commercial fully formulated oil was Mobil 1 5 W-30 and used as-is. The elemental metal composition and preferred functionality of the Mobil 1 5 W-30 (FF oil) are shown in Table 1.

The coupons and 52100 steel cylindrical pins (11 mm length, 6 mm diameter, $R_a \sim 280$ nm) were cleaned in an ultrasonic bath using a light hydrocarbon solvent, and then placed in the Plint high frequency wear tester. The FF oil was poured into the Plint wear tester and the steel pin was laid flat against the disk.

Table 2 Physical parameters tested with FF oil

Time, min	Temperature, °C	Final pressure, MPa	
5	100	180·8	Tribofilm A
60	100	127·3	Tribofilm B
720	100	75·3	Tribofilm C
60	60	137·0	Tribofilm D
60	150	264·6	Tribofilm E

A 220 N load was applied to the pin for the steel samples. The temperature was raised to the desired endpoint and maintained throughout the experiment and the pin was reciprocated with a stroke length of 7 mm at a frequency of 25 Hz (0·35 m s^{-1}). The software monitored the lateral force F_T throughout the experiment through the use of a strain gauge, allowing for a calculation of the coefficient of friction μ. The conditions tested with the FF oil and the resultant pressure after conclusion of the experiment are presented in Table 2. After each experiment, excess oil was removed from the disks using tissue paper and then the samples were rinsed in hexane. The λ ratio was found to be much less than 1, assuring boundary lubrication conditions.[33]

Chemical analysis

Canadian synchrotron radiation facility (CSRF)

Some of the XANES data were obtained at the Canadian synchrotron radiation facility (CSRF),[34] situated at the 1 GeV Aladdin storage ring, University of Wisconsin, Madison. Phosphorus and sulphur K-edge and molybdenum L-edge spectra were obtained on the double crystal monochromator (DCM)[35] covering an energy range of 1500–4000 eV with photon resolution of 0·8 eV. Phosphorus and sulphur L-edge and boron K-edge spectra were obtained on the Grasshopper soft X-ray beamline covering an energy range of 70–900 eV with photon resolution of 0·2 eV. The phosphorus and sulphur K- and L-edge spectra were calibrated using pure unreacted diisobutyl ZDDP. The Mo L-edge was calibrated using MoS_2, while the B K-edge was calibrated using B_2O_3.

The analysed area was about 2×2 mm. The photoabsorption spectra for both the model compounds and samples were recorded in the total electron yield (TEY) mode and fluorescence yield (FY) mode for both surface and bulk sensitivity[36] respectively. All spectra shown in this paper are an average of two scans that were digitally combined and normalised, with a linear background subtracted using the BAN[37] program.

X-ray photoelectron emission microscopy data acquisition was performed using the spectromicroscope for the photoelectron imaging of nanostructures with X-rays

Table 1 Elemental metal composition and functionality of Mobil 1 5 W-30

Element	Additive concentration, ppm	Preferred functionality
Calcium	2500	Detergents
Phosphorus	750	Antiwear, antioxidant
Zinc	900	Antiwear, antioxidant
Molybdenum	90	Antiwear, friction modifier
Boron	70	Part of a detergent, dispersant, antioxidant package
Magnesium	12	Detergent, dispersant

(SPHINX)[38,39] (ELMITEC GmbH) installed on the HERMON beamline using both the low energy grating (LEG), medium energy grating (MEG) and high energy grating (HEG), at the 1 GeV Aladdin storage ring, University of Wisconsin, Madison. The sample is held at a high negative potential (−20 kV) and photoelectrons are accelerated and magnified through electron optics. The magnified photoelectrons are intensified by two microchannel plates and converted into a visible image by a phosphor screen. For details see Refs. 38 and 39.

The authors acquire an image (~180 μm field of view) optimised to give ~0·2 eV resolution at the phosphorus L-edge (for details see Refs. 26, 38 and 39). Image intensity in XPEEM is proportional to the TEY, and the surface sensitivity was limited by the escape depth of the secondary electrons at the phosphorus L-edge (3–5 nm).[40,41] Spectromicroscopy images were taken with a 0·2 eV step size from high energy to low energy. A 100 μm field of view was chosen for the selected area with a resolution of ~200 nm per pixel. The images were combined to produce a three-dimensional data set or spectromicroscopy 'stack'[41] that was analysed to extract detailed chemical information about the tribofilm using aXis2000 software.[41–43] The software allowed for selection of regions of several pixels in size to extract XANES spectra.

Stacks were acquired at the phosphorus L-edge, sulphur L-edge (second order), B K-edge (second order), Mo L-edge (second order), Al L-edge, and Si L-edge using the LEG on the beamline and the O K-edge, Ca L-edge using the MEG of the beamline. Stacks were also attained at the Fe L-edge on the HEG. All useful stacks were analysed for differences in chemistry.

Canadian light source

Supplementary XANES data were obtained at the CLS Inc., affiliated with the University of Saskatchewan, Saskatoon, Canada.

Zinc L-edge, O K-edge, Ca L-edge, C K-edge, Fe L-edge XANES spectra were obtained on the spherical grating monochromator (SGM)[44] capable of covering an energy range of 250–2000 eV with photon resolution of >5000 ($E/\Delta E$).[44] The analysed area was about 1×1 mm. The photoabsorption spectra for both the model compounds and samples were recorded in the TEY mode and FY mode for both surface and bulk sensitivity.[36] The intensity of this beamline is much larger than the Grasshopper at the CSRF, with much better energy resolution above 200 eV.

The zinc L-edge spectra were calibrated using a photoionisation chamber and a Scienta SES 100 photoelectron analyser. The photoionisation spectra of several gas phase standards were used to provide absolute calibration points. Then the photoemission spectra of C 1s, O 1s and W 4f were used to generate calibration points at energies relative to the absolute energies. Three different photoemission peaks were used to confirm the calibration of the electron energy analyser. Both the Fe L-edge and O K-edge XANES data were calibrated using Fe_2O_3. The Ca L-edge XANES was aligned to the literature value of the $2p_{3/2}$ and the $2p_{1/2}$ peaks.[45]

Topography and morphology of substrate

Atomic force microscope (AFM) topography images were recorded for all the samples in air using a Nanoscope IIIa equipped with a Multimode head (Veeco, Santa Barbara, CA). The images were collected in contact force mode with a V shaped silicon nitride cantilever possessing a spring constant of 0·12 N m^{-1}.

Mechanical analysis, evaluation of wear and FIB

The mechanical properties of the substrate and antiwear films were investigated using a Hysitron Triboindenter, equipped with an optical microscope in which a desired area can be chosen in the field of view. This system has the capability to extract mechanical properties with very high force, spatial and depth resolutions. A Berkovich indenter with an elastic modulus E_i between 1000 and 1140 GPa, a Poisson ratio v_i of 0·07 and a tip radius of ~200 nm was used for all indentations. For experimental details see Refs. 46–48, for a schematic see Ref. 48.

Topographic images were obtained with ~2 μN force both before taking an indent and after indenting a region. The quasi-static measurements consisted of increasing the load to a chosen preset value via a constant velocity displacement of the indenter, followed by retraction at the same velocity. The loading process to the preset force, and unloading portion were all monitored. The elastic modulus was extracted using the Oliver–Pharr method[49] from the unloading section of the force–distance (f–d) curve. The films were investigated with a 50 μN maximum preset applied load.

Wear scar widths (WSW) of the steel pins were measured using a calibrated optical Zeiss Axioplan microscope over 10 random regions along the length of the pin. Ten arbitrary regions along each wear scar were averaged, and these values were used as a measure of wear performance.

Rectangular cross-sections of the antiwear films studied by X-PEEM were excised with a focused ion beam (FIB) installed on a LEO 1540XB scanning electron microscope at the Nanofabrication Laboratory, at the University of Western Ontario. The ions used for machining were gallium (Ga^+) with a current of 50 pA for 300 s. The antiwear film thickness was averaged along the cut. Imaging with the SEM was done before and after the FIB milling.

Results and discussion

Chemical analysis

Phosphorus

Previous efforts from the authors have shown that the molecule ZDDP decomposes with temperature and time to form polyphosphates of varying chain length.[5,15,50,51] The cation composition depends on the available sources in the oil additives.[15]

Through studying the P K- and L-edge XANES, local geometry and chemical information of the P containing species can be determined. Figure 1 shows the P K-edge XANES collected in TEY. The P K-edge spectra monitor the transitions of the core P 1s electrons to unoccupied *p*-like valence states. The surface sensitivity for the TEY is ~50 nm, and hundreds of nm in the FY mode.[40] Since the FY probes deeper than the thickness of the films, the FY can be used to provide information about bulk chemistry of the film. The TEY and FY

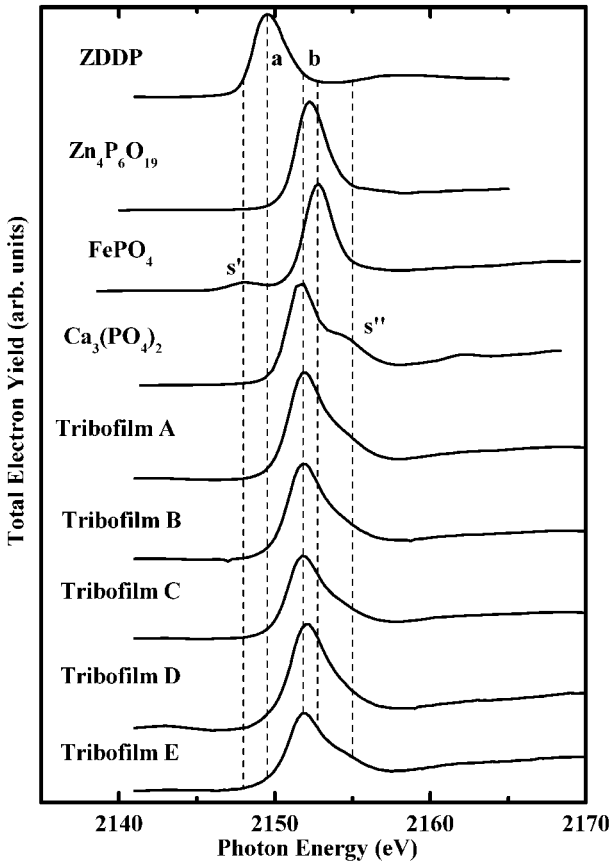

1 Phosphorus K-edge XANES spectra of unreacted ZDDP, model polyphosphates, and tribofilms A–E

spectra show essentially the same features and only the TEY signal is shown.

Figure 1 shows a large energy shift of the white line from the tribofilms (peak b – about 2152 eV) compared to that of ZDDP (peak a – about 2149 eV), indicating a phosphate has formed from the ZDDP precursor. Lack of the pre-edge peak (labelled s′) indicates that no iron phosphate is present on the surface as previously seen on ZDDP derived films[52] (also *see* Fig. 2 for the O K-edge spectrum). Furthermore, a slight difference is observed in the position of the main peak (peak b) of the model compounds between $Ca_3(PO_4)_2$, $Zn_4P_6O_{19}$ and $FePO_4$. Also a post-edge shoulder (labelled s″) is associated with the presence of calcium.

Comparing the spectra of the tribofilms under all the conditions (tribofilms A–E), a polyphosphate has formed, in which the spectra suggests the major cation is Ca, based on the position of the main peak and the significance of the post-edge shoulder (s″). The presence of Ca incorporated into the phosphate network has been alluded to by previous authors[9,12] and corroborated by more conclusive approaches[14,15,17] when a lot of Ca is present in the oil. However, based on the resolution of these spectra, the authors cannot eliminate the possibility of the presence of some Zn phosphate and very small amounts of unreacted ZDDP.

An estimation of P film concentration can be made from the intensity of the FY from the P K-edge XANES,[53] which has been demonstrated to be a reliable measure of the average film thickness assuming the film is composed mostly of phosphate.[31,54] Table 3 presents the average phosphorus concentration for tribofilms

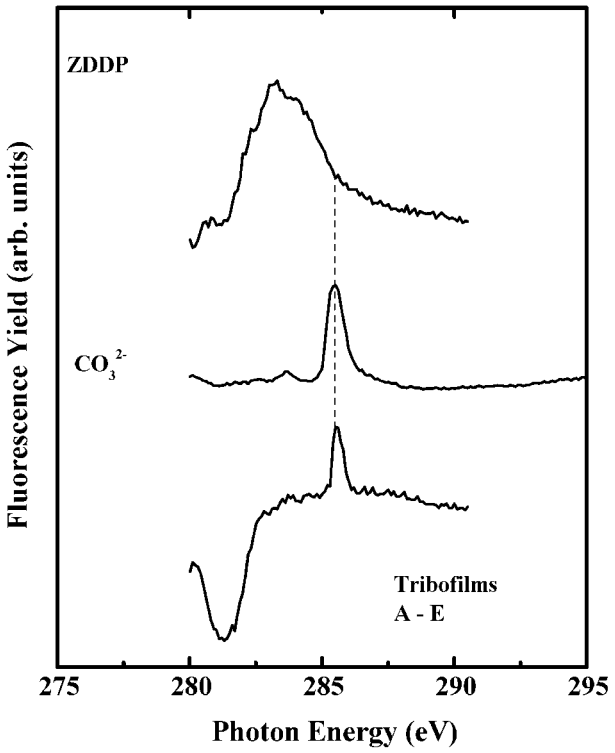

2 C K-edge XANES of representative tribofilms collected in FY mode

A–E. The P concentration remains quite stable with rubbing time ($2–3 \times 10^{16}$ atom cm^{-2}), and from the temperature series the authors cannot deduce a clear trend in P concentration. This differs from a dual additive study involving ZDDP plus antimony dithiocarbamate, where Palacios[55] proposed that higher temperatures generate thicker films. These P areal concentrations are all much thinner than those obtained previously on films made from ZDDP plus one other additive.[15,56]

Deconvolution of the P K-edge XANES has been previously carried out[30,54] to estimate the amount of phosphorus species present as either unreacted ZDDP or polyphosphate, and the procedure can be viewed elsewhere.[57] The results of this method indicate that less than 5% of the P content remains as unreacted ZDDP with the rest being transformed to polyphosphate.

The P L-edge provides better detail of the oxidation and local environment than the P K-edge. The phosphorus L-edge XANES data collected in TEY are presented in Fig. 3. The large spot size (~ 4 mm^2) gives

Table 3 P film concentration of FF oil based on conditions listed in Table 2*

Tribofilm	P film concentration, $\times 10^{16}$ atom cm^{-2}
Tribofilm A	3·1
Tribofilm B	2·4
Tribofilm C	2·8
Tribofilm D	0·52
Tribofilm E	1·5

*The P film concentration is derived from the P K-edge FY intensity.
†Assuming a $Zn_2P_2O_7$ (ρ=3·75 g cm^{-3}) film composition, the film thickness ranges between 40 and 200 Å (Ref. 52).

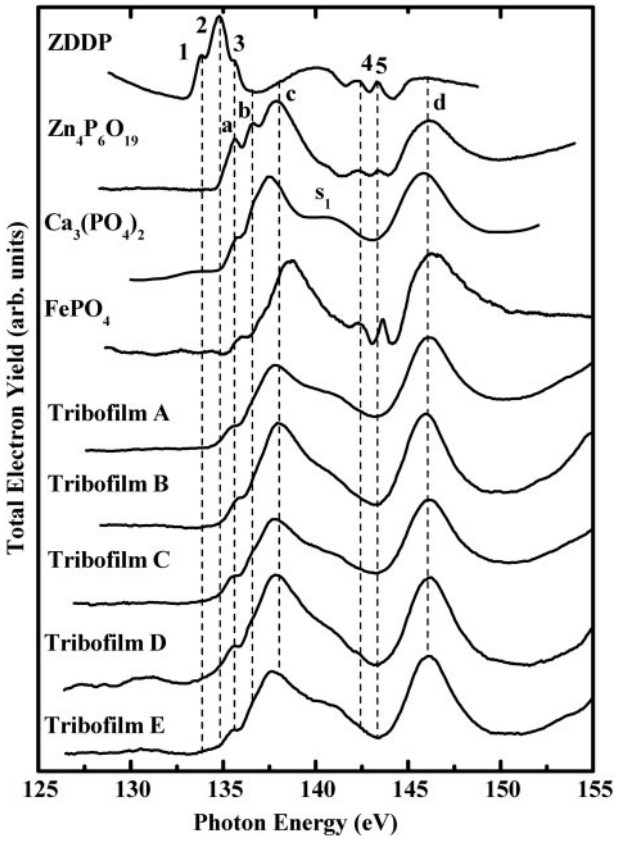

3 Phosphorus L-edge XANES spectra of unreacted ZDDP, model polyphosphates and tribofilms A–E

an average spectrum for the compounds analysed. Figure 3 compares the spectra for several model compounds and tribofilms A–E. The peak assignments for ZDDP and the phosphate model compounds have been given elsewhere.[19] A shift can be observed when comparing calcium, iron and zinc phosphates. The subtle differences in the spectra are caused by the electronegativities of the cation, which result in different antibonding orbital interactions in the different phosphates. The peak positions can be found elsewhere.[19] The main peaks for calcium orthophosphate are shifted by $\sim 0{\cdot}5$ eV to a lower photon energy compared to zinc phosphate, and a broad shoulder (s_1) is present which helps distinguish between calcium and zinc or iron phosphate.

From Fig. 3, based on the shift of the peaks of the tribofilms (peaks a–d) compared to that of ZDDP (peaks 1–3), the authors have determined that a polyphosphate has formed from the decomposition of ZDDP. Based on the alignment of the main peak, and the presence of the shoulder present on all the tribofilms, a Ca phosphate, with some Zn phosphate, seem to be the prevalent species formed, confirming the P K-edge results.

It has been found that the ratio of peaks a/c provides a semiquantitative estimation of the chain length in a phosphate glass.[58] The average a/c ratio was found to be $0{\cdot}54 \pm 0{\cdot}04$ and based on a calibration, it was found that a medium chain polyphosphate (between 10 and 25 P atoms)[30] is formed which is considerably larger than the a/c ratio ($\sim 0{\cdot}20$) found previously when studying the dual additives, ZDDP plus calcium sulphonate (400 TBN) on 52100 steel.[59]

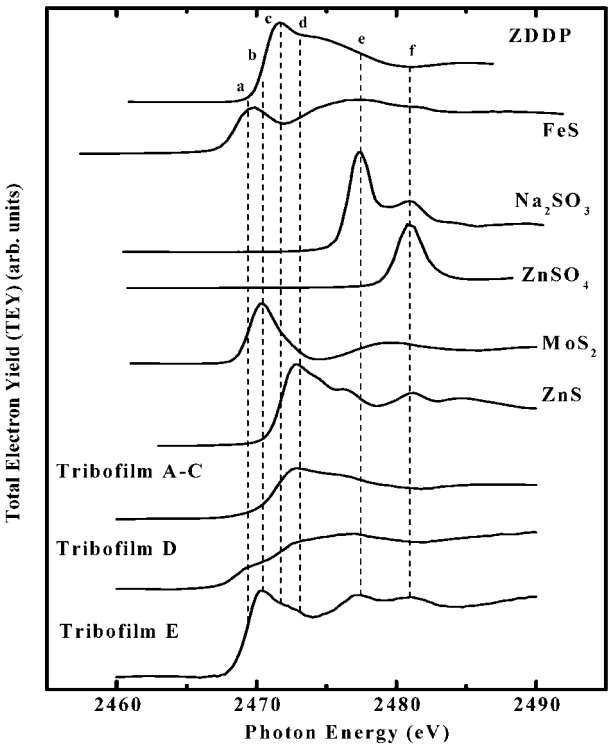

4 S K-edge XANES spectra of unreacted ZDDP, model compounds containing sulphur and tribofilms A–E

Sulphur

The S K-edge XANES of model compounds and tribofilms are shown in Fig. 4. The spectra for the tribofilms made as a function of rubbing time (tribofilms A–C) were found to be almost identical to the spectra for ZnS. Through a deconvolution procedure shown elsewhere,[30,60] the authors can estimate the percentage of species present. Only one peak was fit for MoS_2 and FeS, and another peak for unreacted ZDDP, FeS_2 and ZnS, as the peaks are not well resolved and the energy difference between the compounds is very close to the resolution of the beamline. A summary for the approximate percentages found for each sulphur species is shown in Table 4. It was found that for tribofilms A–C, the prevailing species is the reduced form of sulphur, most likely ZnS, as found in other studies.[19,51] For the lowest temperature studied (tribofilm D), a more significant amount of FeS and MoS_2 was detected. The authors suggest MoS_2 is the dominant species (rather than FeS) and their argument is reinforced in the section on 'Molybdenum'. The presence of FeS is unlikely especially since the film is formed under the mildest temperature (60°C). Usually FeS is formed under extreme conditions and believed to form at high interfacial temperatures, typically greater than ~ 1300°C.[61]

At higher temperatures (tribofilm E), the spectra show increased contributions from MoS_2 and sulphate (feature labelled f). It has been suggested[62] that the presence of sulphate causes an increase in friction due to a higher surface temperature. These spectra are in good agreement with single additive results obtained previously[17,62] indicating that the sulphur species is mostly comprised of a mixture of MoS_2 and ZnS. The deconvoluted intensity of the sulphite species has been observed in a previous report, which resulted from a disproportionantion of a Ca sulphonate detergent.[59]

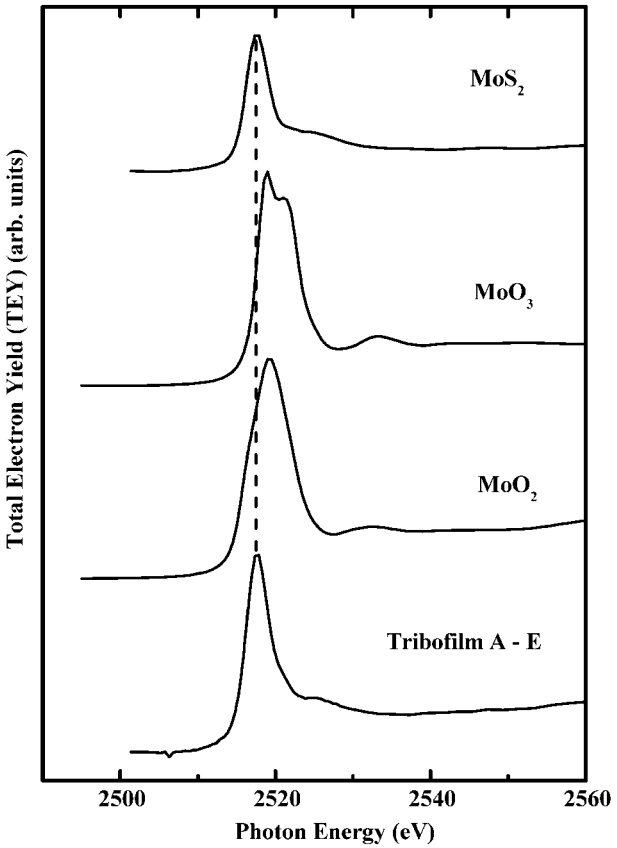

5 Mo L-edge XANES spectra collected in TEY mode comparing model molybdenum compounds and generalised spectrum representing tribofilms A–E

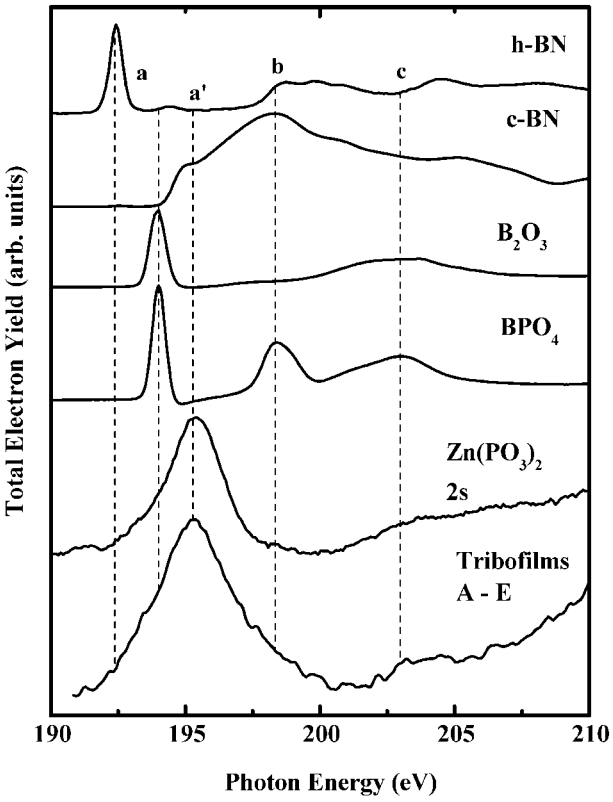

6 B K-edge XANES spectra showing model boron compounds, zinc phosphate (P 2s partially overlaps with B K-edge) and averaged spectrum representing tribofilms A–E

Molybdenum

The molybdenum L_3 ($2p_{3/2}$)-edge XANES is presented in Fig. 5. An averaged spectrum is shown for tribofilms A–E. The single intense peak of MoS_2 (~2517·6 eV) aligns nicely with that of the tribofilms, indicating that the Mo content of the film is present as MoS_2 and no Mo oxides (~2519 eV) are present as the spectra lack the inherent shifts and post-edge features.

The spectrum with the highest intensity (not shown) and lowest noise was for tribofilm E. Evidence for MoS_2 is well documented,[17,19,21,63–67] however the present data suggest that the higher temperatures facilitate the formation of MoS_2 probably due to the higher rate of decomposition of ZDDPs thus providing a surplus of S^{2-} ions as suggested previously.[65]

Boron

The boron chemistry was also investigated by XANES spectroscopy. The K-edge XANES collected in TEY are shown in Fig. 6. The boron model compounds show three distinct features that are correlated to the coordination of the boron atom. Peak a and the broad peak c indicate that boron is associated with trigonal geometry (B_2O_3), while peak (peak b) is correlated to the tetrahedral coordination (BPO_4).[68] Peak a for h-BN is shifted ~2 eV to a lower energy, enabling a distinction between h-BN compared to B_2O_3 and BPO_4. Kasrai *et al.*[68] have shown that BPO_4 normally possesses a tetrahedral geometry, however evidence of trigonal coordination is detected due to surface reconstruction resulting from hydration.

A detailed listing for peak positions of boron containing compounds is given elsewhere,[20] and the interpretation for the peak assignments of the B XANES is also reported elsewhere.[68] The spectra for h-BN and c-BN are included for comparison. The spectral features that align with a′ result from the P 2s of phosphate [$Zn(PO_3)_2$]. However, the B K-edge cross-section is much larger than that of the P L_1-edge (P 2s), thus the B K-edge XANES peaks should be much more intense than the P L_1-edge as shown in the spectra for BPO_4.

No useful B K-edge XANES spectra for the FF oil itself could be acquired. A representative spectrum for the tribofilms is shown and compared to spectra obtained for the model compounds. The very broad weak spectrum for the tribofilms is extremely similar to the P 2s (L_1-edge) spectrum from $Zn(PO_3)_2$. This shows

Table 4 Deconvoluted peak area percentage (%) of sulphur K-edge spectra (see text for detail)

Samples	MoS_2 (2470·25 eV) and FeS (2469·9 eV), %	FeS_2 (2471·3 eV), unreacted ZDDP (2471·8 eV) and ZnS (2472·9 eV), %	SO_3^{2-} (2477·3 eV), %	SO_4^{2-} (2480·8 eV), %
Tribofilms A–C	1·6	98·4	0	0
Tribofilm D	13	87	0	0
Tribofilm E	20	53	21	6

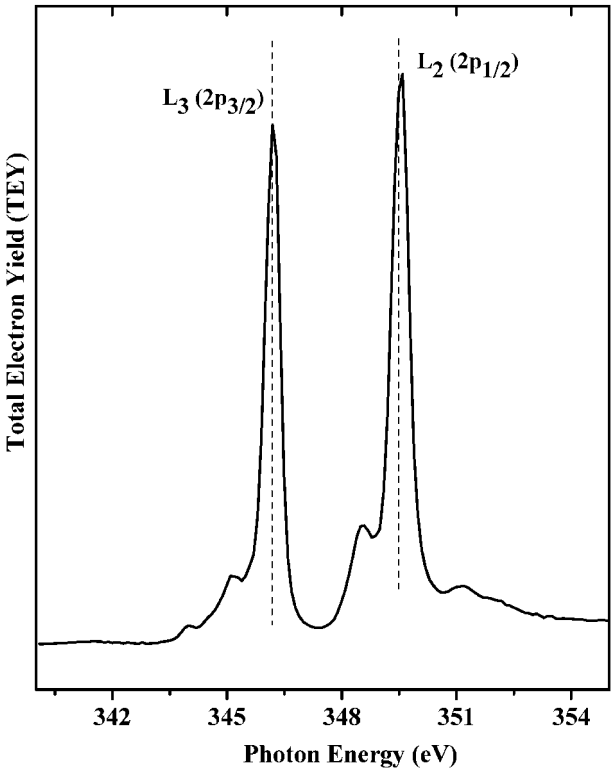

7 Ca L-edge XANES showing representative spectra for tribofilms A–E

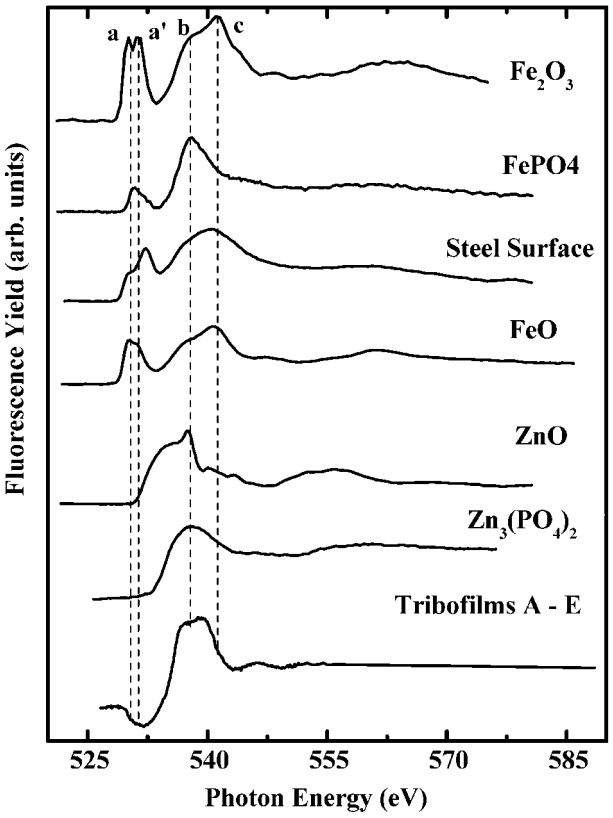

8 O K-edge XANES showing model O compounds and representative spectra for tribofilms A–E collected in FY

that little or no B becomes incorporated into the antiwear film which differs significantly from results obtained on a dual additive study conducted by Zhang *et al.*[20] It is not known where the boron ends up; this is a significant area of active inquiry. The authors are not aware of the chemical nature of B in the FF oil (but the authors do know it is present – *see* Part 2), which can heavily influence its effect on film formation. More studies are needed to help explain this unexpected finding.

Calcium and carbon

The Ca spectra were collected for all samples. The intense L_3 ($\sim$346·2 eV) and L_2 ($\sim$349·6 eV) edges (spin orbit doublets) are easily viewed in Fig. 7. All the tribofilms generated similar spectra. Unfortunately, differences in Ca chemistry are not easy to identify with XANES, as the changes in the XANES spectra with changes in Ca chemistry are very subtle and it is very difficult to distinguish between CaF_2, calcium pyrophosphate [$Ca_2P_2O_7.2H_2O$], calcium carbonate ($CaCO_3$), and calcium whitlockite [$Ca_3(PO_4)_2$].[69]

The authors have also measured the C K-edge XANES (Fig. 2). The carbon contamination on the optics contributes to the complexity of the C characterisation. However, CO_3^{2-} is usually detected in the form of $CaCO_3$, when the initial concentration of the detergent is high, along with a high degree of overbasing.[15]

Oxygen

An O K-edge spectrum collected in FY of the tribofilms is shown in Fig. 8, compared to the O K-edge XANES spectra of model compounds FeO, Fe_2O_3, $FePO_4$, the 52100 substrate, ZnO and $Zn_3(PO_4)_2$. The spectra for the FY were found to be exactly the same as the TEY. This edge has been useful in determining that little Fe is present in the antiwear films.[52]

The Fe compounds show spectral characteristics (pre-edge peaks 'a' and 'a′') that are absent in the spectra of Zn compounds, which can help to differentiate between them. The origin and peak assignments of the O K-edge XANES can be found elsewhere.[70] Briefly, the pre-edge split peaks are transitions from the O 1s to 2p states that are hybridised with the partially filled Fe 3d band that are separated by the ligand field splitting. The pre-edge peaks in the spectra are absent for the Zn model compounds because of the filled 3d orbital. Peaks labelled 'b' and 'c' are attributed to the O 1s to O 2p transition that are hybridised with either the 4s or 4p of Fe or Zn.[70–72]

X-ray absorption near edge structure and X-ray photoelectron spectroscopy (XPS) profiling of films derived from ZDDP show Zn^{2+} as the primary cation near the surface;[52,73] Auger depth analysis[74] confirms Zn in the near surface region, but shows Fe species in the bulk of the films. Because the fluorescence detection technique is a bulk sensitive technique (probing deeper than the film thickness), the evidence reveals that for fully formulated oils, under the conditions tested, significant amounts of iron phosphate or iron oxides are not detected. An intuitive explanation as to why iron oxide is not detected is that before the formation of the tribofilm during sliding contact, the oxide layer is removed and adsorption of ZDDP on the nascent surface then prevents further oxide formation.

Zinc

The Zn L-edge spectra collected in TEY mode are shown in Fig. 9. With the exception of ZnO, all other

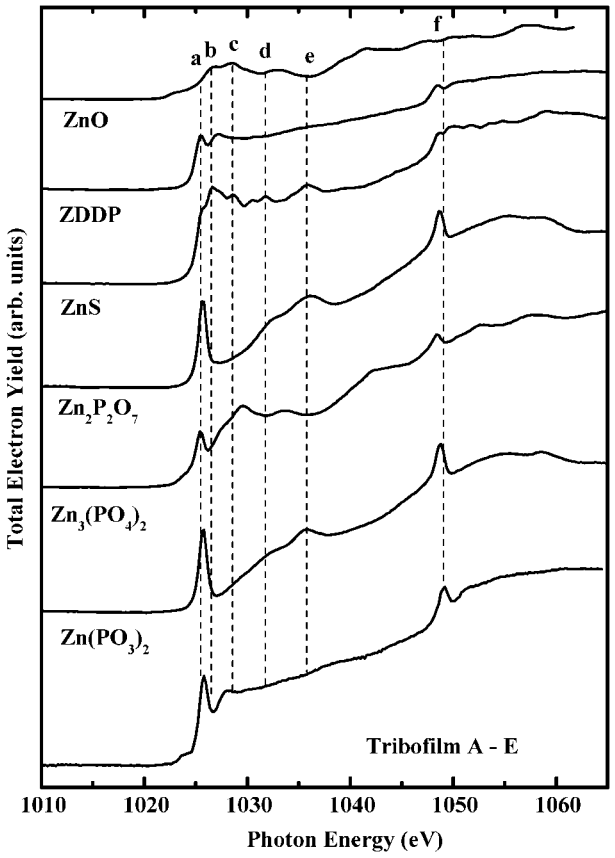

9 Zn L-edge XANES collected in TEY mode comparing model compounds to representative spectra for tribofilms A–E

compounds show intense peaks at $\sim 1025{\cdot}8 \pm 0{\cdot}5$ eV, and this peak is not useful for chemical identification of the Zn species. Based on the spectra, The authors do not see evidence for the formation of ZnO in either the TEY or the FY spectra, which is usually believed to be present as a product of the phosphate reactions.[75] At higher energies, the model compounds have markedly different spectra, which enable the authors to distinguish ZnS from the different phosphates. The rich above edge structure is currently being investigated by density functional theory (DFT) calculations but from a qualitative view point, several observations can be made.[76]

The presence of peaks a (L_3 edge) and c indicates zinc in either the form of zinc phosphate or unreacted ZDDP. Based on the P K-edge XANES, the most intuitive allocation of peaks a, c and f (L_2 edge) are due to zinc phosphate. The presence of ZnS is indicated by the peaks b and d.

Figure 10*a* and *b* show the deconvolution of peak intensity and height of model compounds ZnS and ZDDP. Both compounds were fit in the same manner. An arctangent step function representing the transition of ejected photoelectrons to the continuum has been fitted to the spectra. The Zn $2p_{3/2}$ white line peak and features beyond the edge until the $2p_{1/2}$ white line peak were fitted, while the peak positions and the decay of the arctangent were fixed. All other parameters were allowed to vary.

The relative fraction of each species was calculated by determining the area of the Gaussian peak for that species divided by the total area of all the Gaussian peaks for each zinc species present in the wear scar. The peak height of each feature was calculated from the fitted spectra with the background subtracted. The values obtained from the peak height of the tribofilm were fit in the same manner and compared to the model compounds. A ratio was taken from the remaining peaks to the normalised peak 'A', and the results are summarised in Table 5. Included in the table is the ratio for $Zn_3(PO_4)_2$, $Zn_2P_2O_7$ and $Zn(PO_3)_2$ (fitted spectra not shown).

From the ratios, the peak heights for ZnS are significantly larger than those of the phosphates or ZDDP. This finding can be used as a qualitative fingerprint as well as help to semiquantitatively determine the amount of species present in the tribofilm.

From Table 5, the deconvoluted peak heights give a semiquantitative ratio of ZnS to zinc phosphate in the wear scar (Fig. 10). In total, five peaks were fit (peaks A–E) for ZnS and the tribofilms, and the ratio of integrated heights were compared. Three peaks were fit for zinc phosphates and ZDDP. The averaged peak heights for ZnS was found to range between about 44 and 64% from the normalised peak.

Figure 10*c* shows the deconvoluted spectra for a representative tribofilm. Five peaks were fit for the tribofilm with similar positions and widths to ZnS, based on the features present in the spectra. The weighted heights for all five peaks were found to be $42 \pm 8\%$ of the normalised peak. The presence of peak E is the main evidence for ZnS. Based on the peak heights of the features beyond the white line, the authors modestly estimate the Zn content to be $\sim 78\%$ ZnS. This is the first finding of such nature, as ZnS is normally thought of as a weak contributor to the overall film composition, and Zn is usually associated with P and not S, in strictly ZDDP derived films.[77] These findings are consistent with the S K-edge results.

Total chemical analysis

The XANES results show conclusively that the major chemical species in the films are Ca phosphate, ZnS and MoS_2, with lesser amounts of Zn phosphate. From the XANES results it is very difficult to try to quantify the specific phosphorus content in the film. X-ray photoelectron spectroscopy could be used. However XPS only samples approximately the first 5 nm of the film and Ar^+ etching is required which can potentially change the chemistry of the film.

Energy dispersive X-ray (EDX) spectroscopy was carried out (between 3 and 15 kV), which samples the complete depth profile of the film, and also much of the substrate. Due to the inhomogeneous nature of the film, the distribution of several atomic detected species (Zn, S, Ca and P) is highly variable. Although the EDX peaks are weak because the films are thin, the P atomic

Table 5 Peak ratios of deconvoluted Zn $2p_{3/2}$ L-edge: peaks are normalised to peak A

	A/A	B/A	C/A	D/A	E/A
ZnS	1	0·55	0·49	0·53	0·61
ZDDP	1	0·37	–	–	–
$Zn(PO_3)_2$	1	0·22	–	–	–
$Zn_2P_2O_7$	1	0·16	–	–	–
$Zn_3(PO_4)_2$	1	0·23	–	–	–
Tribofilm	1	0·54	0·37	0·34	0·44

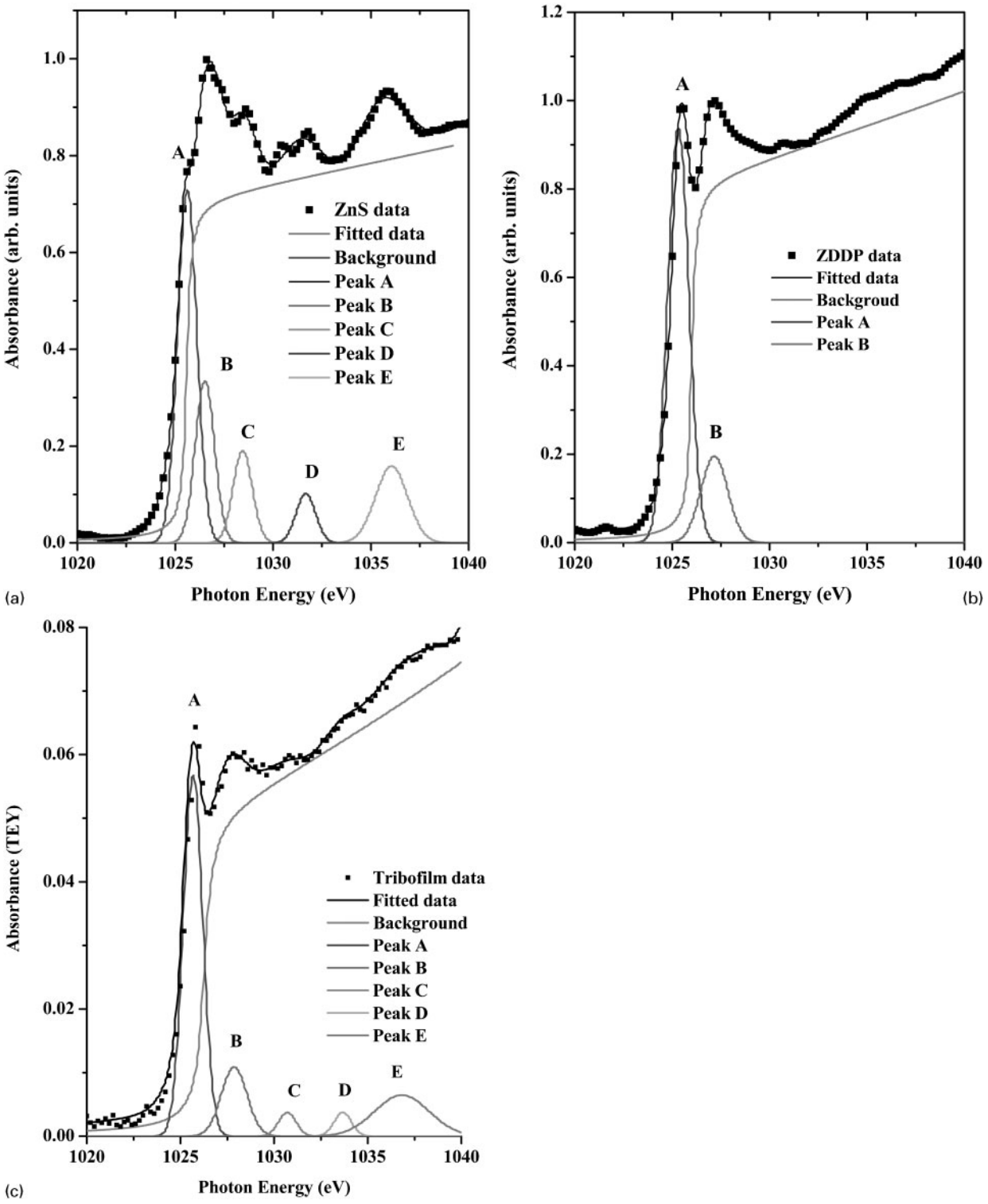

10 Spectral fit of model compounds *a* ZnS and *b* ZDDP and *c* normalised and deconvoluted Zn $2p_{3/2}$ edge of representative spectra for tribofilms A–E: peak allocation and discussion is found in text

percentage was found to be quite steady at $\sim 23 \pm 5$ at.%. Assuming the two main species are Ca phosphate and ZnS (*see* the section on 'Thermal films and mechanism', equation (1)), it is apparent that there has to be more molecules of ZnS than Ca phosphate to achieve this ratio.

Focused ion beam milling was attempted, but due to irregular substrate features and the fact that the steel used is magnetic which distorts the electron beam, poor film edge resolution was obtained and the images were difficult to interpret. From the FIB milling results (not shown), the authors have roughly estimated the thickness to be between 80 and 120 nm. These estimations are comparable to previous values obtained from ZDDP only films[54,56] and films containing ZDDP plus a detergent.[15]

AFM and indentation characterisation

Figure 11 is a representative 75×75 μm AFM height image of the tribofilm B. Two distinct areas are shown,

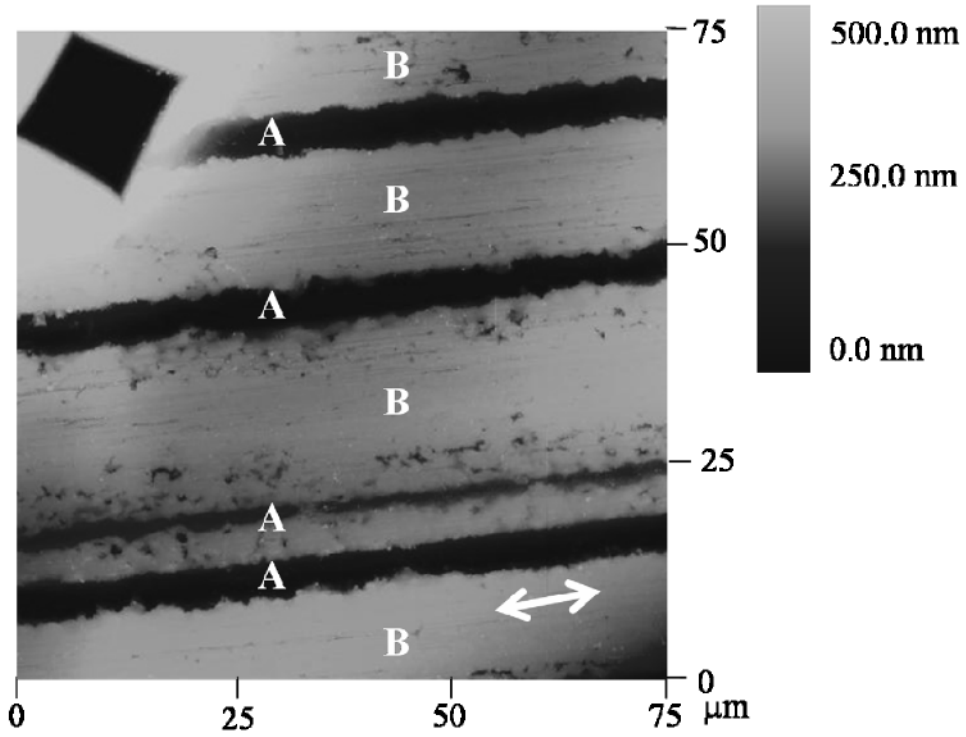

11 Representative 75×75 μm contact AFM image of surface after tribofilm formation: image shown is of tribofilm B; regions of interest are shown (A and B), which relate to mechanical properties, discussed in text

labelled A and B, which will be addressed throughout and the rubbing direction is shown (double sided arrow). Trenches appear, which on average are ~300 nm deep (regions labelled A) and which are believed to result from high pressure contact points, due to unevenness of the steel pin surface and/or unevenness of the coupon. A fiducial marking is shown in the upper right section of Fig. 11. A series of these markings are useful to relocate an area studied with X-PEEM, AFM, EDX (results not shown), and to evaluate the mechanical properties.

Subtle differences arise when comparing the topography of tribofilms from ZDDP only films,[29,31] to ZDDP plus additives,[17,29] to the topography of FF oils. The ZDDP only films and ZDDP plus additives, result in a patchy topography consisting of discontinuous pads, whereas the topography generated from the FF oil appears continuous with the exception of the trenches.

Instrumented nanoindentation was performed on the FF oil samples. Details of the instrumentation, calibration, calculations and assumptions are given elsewhere.[31,78] Topographic images were taken before taking an indent and after indenting a region with the same tip. Force–distance (f–d) curves were taken with loads of 30 μN for the tribofilms, to minimise the influence of the underlying substrate.

The indentation modulus E_s* is a commonly used value to compare the stiffness of the films without prior knowledge of the materials Poisson's ratio, while taking into account the mechanical influence of the indenting tip. Table 6 evaluates the differing mechanical properties of the FF oil and compares these values to experimental values obtained on films made with ZDDP+Ca sulphonate detergent,[29] ZDDP only films and the 52100 steel substrate.[31]

The indentation modulus of region B coincides quite reasonably with ZDDP derived films (*see* Ref. 31) and within the error of the other tribofilms tested. This value is assumed to be a representative modulus for all the FF tribofilms. It is not possible to determine whether any single additive has a significant influence on the indentation modulus versus the final formulated package. However, it is well accepted that the phosphate antiwear pads formed are softer than the steel substrate, thus offering potential to protect the surface by compensating shear stresses and by distribution of localised pressure.

The parallel trenches found in Fig. 11 (region A) exhibit a modulus very comparable to the steel substrate indicating no film formation and corroborating the argument that metal–metal contact is responsible for these trenches.

Table 6 Indentation moduli E_s* of antiwear films formed on tribofilm B, presented with other data pertinent for comparison

	Indentation modulus E_s*, GPa
Steel substrate	218±15
ZDDP pad	103±11
ZDDP+Ca sulphonate detergent (400TBN)	83–90
Region A	226±12
Region B	125±10

*Region B exhibits a characteristic modulus value for the FF oil antiwear film.

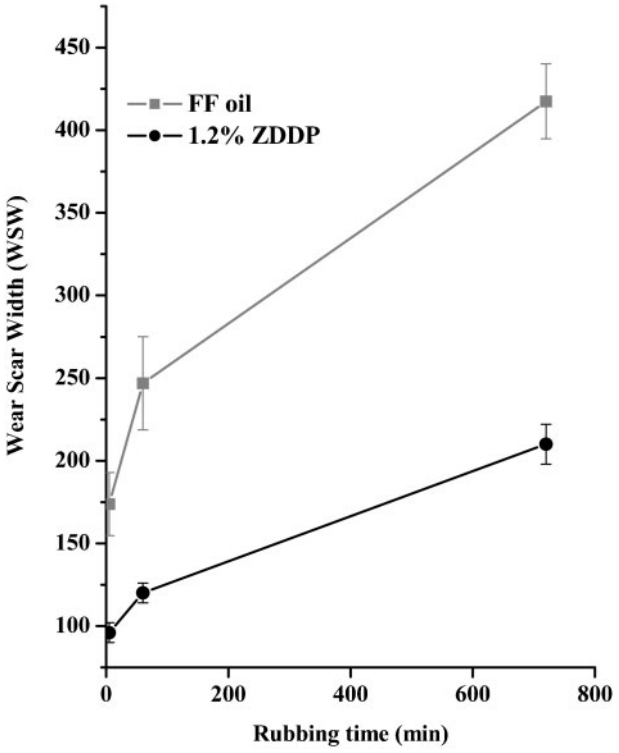

12 Wear scar width as function of rubbing time

X-PEEM

X-ray photoelectron emission microscopy images were acquired for the FF oil antiwear films. Spectra and distribution maps were generated for P, S, B, Ca and Mo. Unfortunately due to poor signal to noise acquisition, meaningful spectra could not be extracted for the Mo L-edge, or the S L-edge. Within the region of interest, no internal chemical differences were found in the spectra of P or Ca; however, as expected, the elemental distribution of Ca was highly correlated with the distribution of P (not shown). Component maps were generated (not shown), but the differences in spectra resulted from a weaker signal, rather than changes in chemistry. The weaker signal is attributed to the trenches observed in the AFM images (Fig. 11), and will not be further discussed. No B K-edge spectra could be obtained from the X-PEEM consistent with the B K-edge XANES spectroscopy.

Friction coefficient and wear scar width

The averaged μ value taken from all the FF oil samples was found to be $0{\cdot}10 \pm 0{\cdot}01$ calculated from a normal force F_N of 220 N. This value is typical for the boundary lubrication regime of ZDDP films formed on steel.[79]

The time dependent wear scar widths (WSWs) for the films formed from FF oils are compared to previous results from only ZDDP are given in Fig. 12 (tribofilms A–C). There is an evident increase in the amount of wear from ZDDP to the FF oils. Consistent with previous results, adding a detergent or dispersant will increase the WSW appreciably from using just ZDDP itself.[15,59] No conclusions could be made from the temperature dependent measurements.

Thermal films and mechanism

The authors attempted to make thermally prepared films by suspending the steel coupons in the FF oil for $\sim$24 h. The temperature regime at which these were prepared ranged from 150 to 185°C. Fuller *et al.*[80] have reported the formation of thick phosphate films under these conditions using just ZDDP in oil. After rinsing the residual oil off the sample with hexanes, no useful spectra could be acquired for any of the edges studied in this paper. No significant thermal films were found at 185°C.

Assuming the film formation from FF oils require much higher decomposition temperatures than for ZDDPs alone, the authors would expect that film formation and growth will be slower than ZDDPs, which would help rationalise the larger WSW.

From the previous sections, the authors recognise that the tribofilm consists mainly of a medium chained Ca polyphosphate (with some Zn phosphate) coexisting with ZnS and MoS_2. Consistent with previous literature on ZDDP plus a Ca dispersant film, the main phosphate species formed is Ca phosphate (with some $CaCO_3$) and not Zn phosphate.[15] However, from the Zn L-edge, the authors have estimated $\sim$78% of the Zn content to be present as ZnS, and thus attributing $\sim$22% of the remaining Zn content to be Zn phosphate and unreacted ZDDP. This behaviour can be rationalised within the hard and soft acid and bases (HSAB) principle previously applied to polyphosphates.[75] Since there is a large amount of Ca (Table 1), and since Ca^{2+} is a harder acid than Zn^{2+}, there is a stronger affinity for formation of Ca phosphate as opposed to Zn phosphate. Furthermore, S^{2-} is a soft base, which would have a tendency to polar covalently bond with a soft Lewis acid, namely Zn^{2+}.

The HSAB principle reflects tabulated thermodynamic properties (Table 7),[81] which have been used previously for film composition studies.[57] In the presence of comparable amounts of Zn, Ca, S and PO_4^{3-}, the authors can write

$$3CaS_{(s)} + Zn_3P_4O_{13(s)} \rightarrow 3ZnS_{(s)} + Ca_3P_4O_{13(s)} \quad (1)$$

Since the Gibbs free energy of formation ΔG_f° for many compounds is not known, the standard enthalpy of formation ΔH_f° can be used as an estimation for ΔG_f°, as the difference is typically quite small (*see* Table 7). Using ΔH_f° as a measure of ΔG_f°, the reaction shown (equation (1)) is strongly negative (−441 kJ), therefore, a high percentage of Ca phosphate and ZnS is expected. Nearly all the O is tied up as phosphate. Other O species could be Fe_2O_3 or CaO, but phosphates are thermodynamically very stable. Mo^{4+} is known to be a soft acid,[21] which facilitates the formation of MoS_2 as long

Table 7 Standard enthalpies of formation ΔH_f° and Gibbs free energy of formation ΔG_f° for selected substances

Substance	ΔH_f°, kJ mol^{-1}	ΔG_f°, kJ mol^{-1}
$ZnO_{(s)}$	−348·28	−318·30
$ZnS_{(s)}$ (sphalerite)	−192·63	–
$ZnS_{(s)}$ (wurtzite)	−205·98	−201·29
$Zn_2(P_2O_7)_{(s)}$	−2510·4	–
$Zn_3(PO_4)_{2(s)}$	−2892·4	–
$Zn_3P_4O_{13(s)}$	−4479·4	–
$CaO_{(s)}$	−635·09	−604·03
$CaS_{(s)}$	−482·4	−477·4
$Ca(PO_3)_{2(l)}$	−2456·0	–
$Ca_3(PO_4)_{2(s)}$	−4109·9	−3875·5
$Ca_3P_4O_{13(s)}$	−5749·0	–
$MoS_{2(s)}$	−235·1	−225·9

as S^{2-} is available. This is again expected by the considerable ΔG_f°, for MoS_2 (Table 7).

One of the most surprising finds was the lack B within the antiwear pads. B is not incorporated into the film, as seen in exclusive studies involving ZDDP + B. This leads to many questions:

(i) what happens if all the B containing components are removed
(ii) does the molecule in which B is incorporated, plays a more significant role than B itself?

A more comprehensive study is needed to rationalise these findings.

Conclusions

In this paper, chemical analyses have shown that FF oils exhibit novel chemistry which has not been previously observed in studies involving individual additives. A comparative study has shown as follows.

1. Medium chain Ca phosphates are the predominant species present.

2. One of the surprising findings of this study was the role of Zn. ZnS has been formed as the primary zinc and sulphur species, under the non-extreme conditions. Approximately 78% of the Zn content was estimated to be present as ZnS. The remaining 22%Zn has been identified to be Zn phosphate. Unreacted ZDDP has been ruled out as a possibility based on the P K-edge findings. Furthermore, the authors have found that at higher temperatures other sulphur species are generated, as appreciable amounts of MoS_2 as well as SO_3^{2-} and SO_4^{2-} have been detected.

3. Another interesting observation was that no B was detected in the film.

4. Energy dispersive X-ray spectroscopy was carried out to estimate the elemental composition of the film. P was found to be evenly distributed at $\sim$23%.

5. A thermodynamic assessment (through a plausible assumption that ΔH_f° approximates to ΔG_f°) shows spontaneous formation of Ca phosphate and ZnS, which are the main components observed experimentally.

6. Atomic force microscopy shows a continuous film with the exception of 300 μm trenches which are believed to originate from metal–metal contact. Two regions were found with differing mechanical properties. The trenches possessed an indentation modulus similar to that of the steel substrate, and the film, although not chemically homogenous, exhibited a fairly reproducible indentation modulus of 125 ± 10 GPa.

7. The WSW for the FF oil appears to be very substantial, consistent with the lack of thermal decomposition up to 185°C, and relatively thin films.

The implications of this study are that ZDDP does not act fully as an antiwear agent in FF oil (in the form of Zn phosphate), and possibly only facilitates the initialisation of film formation. Once the onset of film formation occurs, a ZnS and Ca phosphate film grow based on availability of cations present and in agreement with the chemical hardness predictions. These results and suggestions might be helpful in developing a better understanding of the engine tribochemical and mechanical properties.

Acknowledgements

The authors would like to thank Mr Phil Shaw and Mr Brian Dalrymple of the Physics Machine Shop, Mr Gord Wood of the Earth Sciences Department and Dr. Leighton Coatsworth (all from the University of Western Ontario) for useful discussions and technical support. The authors would like to thank Dr Wayne Chang and the rest of the staff at Surface Science Western (SSW) for assistance in acquiring the SEM/EDX data and Dr Todd Simpson from the Nanofabrication Laboratory for assistance in acquiring the FIB/SEM results. The research described in this manuscript was performed partially at the Canadian Light Source, which is supported by NSERC, NRC, CIHR and the University of Saskatchewan. The authors are also grateful to Dr Astrid Jürgensen from the Canadian Synchrotron Radiation Facility (CSRF), University of Wisconsin, Madison, for her technical support, and the National Science Foundation (NSF) for supporting the SRC under grant no. DMR-0537588. This work was financially supported by the Natural Sciences and Engineering Research Council of Canada (NSERC), General Motors of Canada Ltd, General Motors R & D Center and by the National Research Council of Canada (NRC) which supports the Canadian Synchrotron Radiation Facility at the Aladdin ring in Stoughton, Wisconsin.

References

1. T. Mang and W. Dresel (eds.): 'Lubricants and lubrication'; 2001, Mannheim, Wiley-VCH.
2. Z. Pawlak: 'Tribochemistry of lubricating oils'; 2003, Amsterdam, Elsevier.
3. K. Inoue and H. Watanabe: *ASLE Trans.*, 1982, **26**, 189.
4. H. Spikes: *Tribol. Lett.*, 2004, **17**, 469.
5. M. A. Nicholls, T. Do, P. R. Norton, M. Kasrai and G. M. Bancroft: *Tribol. Int.*, 2005, **38**, 15.
6. A. J. Gellman and N. D. Spencer: *Proc. Inst. Mech. Eng.*, 2002, **216**, 443.
7. K. Fujita and H. A. Spikes: *Proc. Inst. Mech. Eng.*, 2004, **218**, 265.
8. S. Fields: *Tribol. Lubricat. Technol.*, 2005, **61**, 25.
9. P. Kapsa, J. M. Martin, C. Blanc and J. M. Georges: *Trans. ASME*, 1981, **103**, 486.
10. J. A. McGeehan, E. S. Yamaguchi and J. Q. Adams: *SAE Tech. Paper Ser.*, 1985, **852133**, 1.
11. Y. Yamada, J. Igarashi and I. Kiyoshi: *Lubricat. Eng.*, 1992, **48**, 511.
12. P. A. Willermet, D. P. Dailey, R. O. Carter III, P. J. Schmitz, W. Zhu, J. C. Bell and D. Park: *Tribol. Int.*, 1995, **28**, 163.
13. A. B. Vipper, S. J. Cook, A. K. Karaulov, D. J. Moreton, O. A. Mischuk and R. Leahy: *Lubricat. Sci.*, 1997, **9**, 207.
14. Z. Yin, M. Kasrai, M. Fuller, G. M. Bancroft, K. Fyfe, M. L. Colaianni and K. H. Tan: *Wear*, 1997, **202**, 192.
15. Y. Wan, M. L. Suominen Fuller, M. Kasrai, G. M. Bancroft, K. Fyfe, J. R. Torkelson, Y. F. Hu and K. H. Tan: Effects of detergent on the chemistry of tribofilms from ZDDP: Studied by X-ray absorption spectroscopy and XPS: In Dawson D, Priest M, Dalmaz G, Lubrecht AA, eds, Boundary and Mixed Lubrication: Science and Applications volume 40. Amsterdam, Netherlands: Elsevier Science, B.V. 2002, pp. 155–166.
16. S. H. Roby, E. S. Yamaguchi, M. M. Francisco and S. G. Ruelas: *Tribol. Trans.*, 2004, **47**, 517.
17. G. Pereira, A. Lachenwitzer, D. Munoz-Paniagua, M. Kasrai, P. R. Norton, T. W. Capehart, T. A. Perry and Y.-T. Cheng: Nanoscale chemistry and mechanical properties of tribofilms on an Al–Si alloy (A383): Interaction of ZDDP, calcium detergent and molybdenum friction modifier. Tribology–Materials, Surface & Interfaces 2007, **1**, 1–14.
18. F. T. Barcroft and D. Park: *Wear*, 1986, **108**, 213.
19. M. Suominen-Fuller, M. Kasrai and G. M. Bancroft: in 'Advanced series in physical chemistry: part 2', (ed. T. K. Sham), Vol. 12B; 2002, Singapore, World Scientific Publishing Co.
20. Z. Zhang, E. S. Yamaguchi, M. Kasrai and G. M. Bancroft: *Tribol. Trans.*, 2004, **47**, 527.
21. M. I. de Barros, J. Bouchet, I. Raoult, T. Le Mongne, J. M. Martin, M. Kasrai and Y. Yamada: *Wear*, 2003, **254**, 863.
22. E. R. Braithwaite and A. B. Greene: *Wear*, 1978, **26**, 405.

23. J. Stohr: 'NEXAFS spectroscopy'; 1996, Berlin, Springer.
24. G. M. Bancroft: *Can. J. Chem.*, 2004, **82**, 1028.
25. S. Bec and A. Tonck: in 'Tribology series: lubricants and lubrication', (ed. D. Dowson), Vol. 30; 1996, Amsterdam, Elsevier.
26. M. A. Nicholls, P. R. Norton, G. M. Bancroft, M. Kasrai, T. Do, B. H. Frazer and G. de Stasio: *Tribol. Lett.*, 2003, **17**, 205.
27. O. L. Warren, J. F. Graham, P. R. Norton, J. E. Houston and T. A. Michalske: *Tribol. Lett.*, 1998, **4**, 189.
28. J. F. Graham, C. McCague and P. R. Norton: *Tribol. Lett.*, 1999, **6**, 149.
29. M. A. Nicholls, G. M. Bancroft, P. R. Norton, M. Kasrai, G. de Stasio, B. H. Frazer and L. M. Wiese: *Tribol. Lett.*, 2004, **17**, 245.
30. G. Pereira, A. Lachenwitzer, M. A. Nicholls, M. Kasrai, P. R. Norton and G. de Stasio: *Tribol. Lett.*, 2005, **18**, 411.
31. G. Pereira, D. Munoz-Paniagua, A. Lachenwitzer, M. Kasrai, P. R. Norton, T. W. Capehart, T. A. Perry and Y.-T. Cheng: *Wear*, 2006, **262**, 461.
32. Y. B. Guo and C. R. Liu: *J. Manuf. Sci. Eng.*, 2002, **124**, 1.
33. I. M. Hutchings: 'Tribology: friction and wear of engineering materials'; 1992, Boca Raton, FL, CRC Press.
34. G. M. Bancroft: *Can. Chem. News*, 1992, **44**, 15.
35. B. X. Yang, F. H. Middleton, B. G. Olsson, G. M. Bancroft, J. M. Chen, T. K. Sham, K. Tan and D. J. Wallace: *Rev. Sci. Instr.*, 1992, **63**, 1355.
36. M. Kasrai, Z. Yin, G. M. Bancroft and K. Tan: *J. Vacuum Sci. Technol. A*, 1993, **11A**, 2694.
37. T. Tyliszczak: BAN, McMaster University, Canada, unpublished program.
38. B. H. Frazer, M. Girasole, L. M. Wiese, T. Franz and G. de Stasio: *Ultramicroscopy*, 2004, **99**, 87.
39. B. Frazer, B. Gilbert, B. Sonderegger and G. de Stasio: *Surf. Sci.*, 2003, **537**, 161.
40. M. Kasrai, W. N. Lennard, R. W. Brunner, G. M. Bancroft, J. A. Bardwell and K. H. Tan: *Appl. Surf. Sci.*, 1996, **99**, 303.
41. C. Jacobsen, S. Wirick, G. Flynn and C. Zimba: *J. Microsc.*, 2000, **197**, 173.
42. L. M. Croll, J. F. Britten, C. Morin, A. P. Hitchcock and H. D. H. Stöver: *J. Synchr. Radiat.*, 2003, **10**, 265.
43. A. Hitchcock, P. Hitchcock, C. Jacobsen, C. Zimba, B. Loo, E. Rotenberg, J. Denlinger and R. Kneedler: available at: http://unicorn.mcmaster.ca/aXis2000.html
44. B. W. Yates, Y. F. Hu, K. H. Tan, G. Retzlaff, R. G. Cavell, T. K. Sham and G. M. Bancroft: *J. Synchr. Radiat.*, 2000, **7**, 296.
45. A. C. Thompson, D. T. Attwood, E. M. Gullikson, M. R. Howells, J. B. Kortright, A. L. Robinson, J. H. Underwood, K.-J. Kim, J. Kirz, I. Lindau, P. Pianetta, H. Winick, G. P. Williams and J. H. Scofield: 'X-ray data booklet'; 2001, Berkeley, CA, Lawrence Berkeley National Laboratory.
46. A. C. Lund, A. M. Hodge and C. A. Schuh: *Appl. Phys. Lett.*, 2004, **85**, 1362.
47. C. A. Schuh, A. C. Lund and T. G. Nieh: *Acta Mater.*, 2004, **52**, 5879.
48. C. A. Schuh, J. K. Mason and A. C. Lund: *Nature Mater.*, 2005, **4**, 617.
49. W. C. Oliver and G. M. Pharr: *J. Mater. Res.*, 1992, **7**, 1564.
50. M. Fuller, Z. Yin, M. Kasrai, G. M. Bancroft, E. S. Yamaguchi, P. R. Ryason, P. A. Willermet and K. H. Tan: *Tribol. Int.*, 1997, **30**, 305.
51. Z. Yin, M. Kasrai, M. Fuller, G. M. Bancroft, K. Fyfe and K. H. Tan: *Wear*, 1997, **202**, 172.
52. G. Pereira, A. Lachenwitzer, D. Munoz-Paniagua, M. Kasrai, P. R. Norton, M. Abrecht and G. de Stasio: *Tribol. Lett.*, 2006, **23**, 109.
53. M. L. Suominen Fuller, L. R. Fernandez, G. R. Massoumi, W. N. Lennard and M. Kasrai: *Tribol. Lett.*, 2000, **8**, 187.
54. G. Pereira, A. Lachenwitzer, M. Kasrai, P. R. Norton, T. W. Capehart, T. A. Perry, Y.-T. Cheng, B. Frazer and G. de Stasio: A multi-technique characterization of ZDDP antiwear films formed on Al(Si) alloy (A383) under various conditions. Tribology Letters 2007; 26: 103–117.
55. J. M. Palacios: *Wear*, 1987, **114**, 41.
56. Z. Zhang, E. Yamaguchi, M. Kasrai and G. M. Bancroft: *Tribol. Lett.*, 2005, **19**, 211.
57. M. A. Nicholls, P. R. Norton, G. M. Bancroft and M. Kasrai: *Wear*, 2004, **257**, 311.
58. Z. Yin, M. Kasrai, G. M. Bancroft, K. H. Tan and X. Feng: *Phys. Rev. B*, 1995, **51B**, 742.
59. M. Kasrai, M. Suominen Fuller, G. M. Bancroft, E. Yamaguchi and P. R. Ryason: *Tribol. Trans.*, 2003, **46**, 543.
60. G. P. Huffman, S. Mitra, F. E. Huggins, N. Shah, S. Vaidya and F. Lu: *Energ. Fuels*, 1991, **5**, 574.
61. M. N. Najman, M. Kasrai and G. M. Bancroft: *Tribol. Lett.*, 2003, **14**, 225.
62. M. Kasrai, J. N. Cutler, G. Canning, G. M. Bancroft and K. H. Tan: *Tribol. Trans.*, 1998, **41**, 69.
63. M. Muraki and H. Wada: in 'Lubricants and lubrication', (ed. D. Dowson *et al.*), Vol. 30; 1995, Amsterdam, London, New York, Tokyo, Elsevier.
64. M. Muraki, Y. Yanagi and K. Sakaguchi: *Tribol. Int.*, 1997, **30**, 69.
65. M. I. de Barros' Bouchet, J. M. Martin, T. Le-Mogne and B. Vacher: *Tribol. Int.*, 2005, **38**, 257.
66. M. I. de Barros Bouchet, J. M. Martin, T. Le Mongne, P. Bilas, B. Vacher and Y. Yamada: *Wear*, 2005, **258**, 1643.
67. S. Bec, A. Tonck, J. M. Georges and G. W. Roper: *Tribol. Lett.*, 2004, **17**, 797.
68. M. Kasrai, M. E. Fleet, S. Muthupari, D. Li and G. M. Bancroft: *Phys. Chem. Miner.*, 1998, **25**, 268.
69. C. J. Buckley, S. J. Bellamy, X. Zhang, G. Dermody and S. Hulbert: *Rev. Sci. Instr.*, 1995, **66**, 1322.
70. F. M. de Groot, M. Grioni, J. C. Fuggle, J. Ghijsen, G. A. Sawatzky and H. Petersen: *Phys. Rev. B*, 1989, **40B**, 5715.
71. M. Pollak, M. Gautier, N. Thromat, S. Gota, W. C. Mackrodt and V. R. Saunders: *Nucl. Instr. Meth. Phys. Res. B*, 1995, **97B**, 383.
72. Z. Y. Wu, S. Gota, F. Jollet, M. Pollak, M. Gautier-Soyer and C. R. Natoli: *Phys. Rev. B*, 1997, **55B**, 2570.
73. Z. Zhang, E. Yamaguchi, M. Kasrai, G. M. Bancroft, X. Liu and M. E. Fleet: *Tribol. Lett.*, 2005, **19**, 221.
74. J. M. Martin, C. Grossiord, T. Le Mogne, S. Bec and A. Tonck: *Tribol. Int.*, 2001, **34**, 523.
75. J. M. Martin: *Tribol. Lett.*, 1999, **6**, 1.
76. G. Pereira, Y. M. Yiu, Y. Li, A. Lachenwitzer, M. Kasrai, G. M. Bancroft, P. R. Norton, T.-K. Sham, T. Regier, R. Blyth, J. Thompson, Y. Hu and L. Zuin: 2006, in preparation.
77. H. Spedding and R. C. Watkins: *Tribol. Int.*, 1982, **99**, 9.
78. M. A. Nicholls, P. R. Norton, G. M. Bancroft, M. Kasrai, T. Do, B. H. Frazer, G. de Stasio: *Tribol. Lett.*, 2003, **17**, 205.
79. C. Grossiord, J. M. Martin, T. Le Mogne and T. Palermo: *Tribol. Lett.*, 1999, **6**, 171.
80. M. L. Suominen-Fuller, M. Kasrai, G. M. Bancroft, K. Fyfe and K. H. Tan: *Tribol. Int.*, 1998, **31**, 627.
81. D. D. Wagman, W. H. Evans, V. B. Parker, R. H. Schumm, I. Halow, S. M. Bailey, K. L. Churney and R. L. Nuttall: *J. Phys. Chem. Ref. Data*, 1982, **11**, (Suppl. 2), 392.